NANO LETTERS

pubs.acs.org/NanoLett Letter

Observation of Microscopic Domain Effects in the Metal–Insulator Transition of Thin-Film $NdNiO_3$

Lucy S. Nathwani, Anne Ruperto, Ashvini Vallipuram, Abigail Y. Jiang, Grace A. Pan, Dan Ferenc Segedin, Ari B. Turkiewicz, Charles M. Brooks, Jarad A. Mason,* Qichen Song,* and Julia A. Mundy*

Cite This: *Nano Lett.* 2026, 26, 4027–4033 Read Online

ACCESS | Metrics & More | Article Recommendations | Supporting Information

ABSTRACT: Perovskite oxides display correlated electrical, magnetic, and thermal properties that can be further tuned in the thin-film limit, making them contenders for next-generation electronics. Measuring thermal transport in thin films is challenging, because traditional techniques are dominated by the substrate. Here, frequency-domain thermoreflectance (FDTR) of an epitaxial $NdNiO_3$ thin film reveals a sharp change in out-of-plane thermal conductivity across the metal–insulator transition. Complementary frequency-domain photoreflectance (FDPR) reveals a large change in ambipolar diffusivity of photoexcited carriers. While the in-plane electrical resistance shows large hysteresis, out-of-plane thermal and charge transport shows negligible hysteresis. We attribute this discrepancy to anisotropy in the percolation of nanoscale domains across the transition as the film thickness approaches the domain length scale. We establish FDTR and FDPR as sensitive probes of quantum material phase transitions and highlight $NdNiO_3$ for thermal control and memory applications.

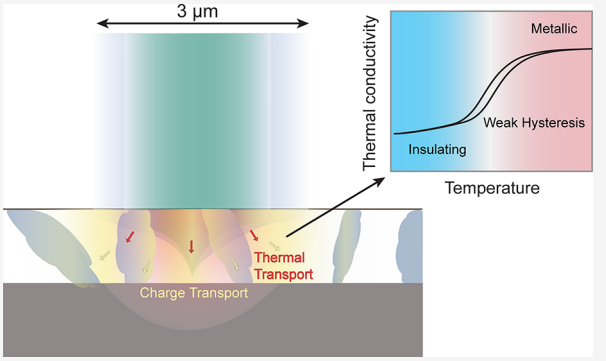

KEYWORDS: *hysteresis, microscopic domains, metal–insulator transitions, thermal transport, charge transport*

As the demand for miniaturized, energy-efficient electronics grows, materials that undergo temperature-driven metal–insulator transitions (MIT) have emerged as candidates for next-generation technologies, including thermal switches for heat regulation, smart windows for thermochromic glazing, nonvolatile memristors for data storage, and neuromorphic computing elements for brain-inspired computing.[1−4] Among these, rare-earth perovskite nickelates, $RNiO_3$ (R = La, Pr, Nd...), are model systems due to their highly tunable phase transitions.[5−8] In particular, neodymium nickelate, $NdNiO_3$, undergoes a first-order phase transition from a paramagnetic metallic state to an antiferromagnetic insulating state, with a concomitant change in the crystal structure at the highest temperature of the $RNiO_3$ series. It exhibits thermal hysteresis due to percolation across domains that emerge during the transition.[9−11] In single crystal $NdNiO_3$, this transition occurs near 200 K. However, in the thin-film limit, the transition temperature can be tuned through epitaxial strain and film thickness,[5,12−15] making it highly adaptable for integration into electronic devices. While most studies have focused on the electrical and magnetic properties of thin film $NdNiO_3$, its thermal properties are highly relevant for its practical applications in devices. Fully exploiting these materials in next-generation devices, however, requires an understanding of anisotropic charge and heat transport at the nanoscale, particularly as the thickness of the film approaches the length scales of domain formation during the phase transition.

Measuring thermal transport in ultrathin films remains challenging due to the limited sensitivity of conventional bulk techniques, as traditional measurements of thermal conductivity using an applied heat source and a voltage measurement are dominated by substrate contributions.[16] While 3ω techniques offer improved sensitivity to thin films, they require complex and invasive sample preparation and lack spatial resolution.[17] Noncontact optical reflectance-based techniques provide an alternative avenue that addresses these limitations.[18] In particular, frequency-domain thermoreflectance (FDTR)[19,20] is capable of measuring the thermal conductivity of films as thin as several tens of nanometers, while requiring only minimal sample preparation (i.e., depositing a metallic transducer). FDTR can even measure thermal transport in monolayer materials like graphene, depending on the film composition and

Received: September 8, 2025
Revised: February 27, 2026
Accepted: March 2, 2026
Published: March 16, 2026

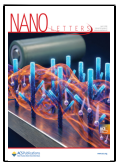

https://doi.org/10.1021/acs.nanolett.5c04522
Nano Lett. 2026, 26, 4027–4033

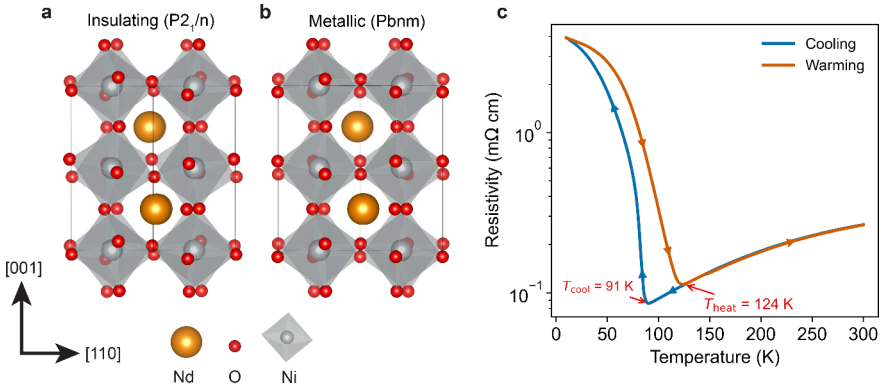

Figure 1. (a) Distorted perovskite structure of $NdNiO_3$ in the insulating phase. (b) The structure in the metallic phase. The changes in octahedral tilts drive the transition.[7] (c) Temperature-dependent resistance capturing the MIT (see SI). T_{MIT} is 91 K during cooling and 124 K during heating. The film is 57.5 nm (150 unit cells) thick in the $(001)_{PC}$ direction, grown on $LaAlO_3$ $(100)_{PC}$.

the substrate,[21,22] and it can be used to map thermal properties with micrometer resolution (Figure S4). The same optical setup without a transducer layer can be used to perform frequency-domain photoreflectance (FDPR), further allowing the charge and thermal transport to be probed simultaneously.[23] Additionally, FDTR is particularly sensitive to the cross-plane thermal conductivity. Scanning thermal microscopy (SThM) techniques have been used to measure the cross-plane thermal conductivity at higher spatial resolution, but these techniques require specialized sample preparation and calibration to gain sensitivity to multiple sample thicknesses simultaneously.[24] With FDTR and FDPR, we can obtain ambipolar diffusivity with no sample preparation and thermal conductivity by depositing only a transducer layer.

In this work, we use FDTR to measure the thermal conductivity of a 57.5 nm thick epitaxial $NdNiO_3$ film grown on a $LaAlO_3$ substrate across its metal−insulator transition, the thinnest such epitaxial oxide measured with FDTR to date. While we observe strong hysteresis in the in-plane electrical transport, consistent with prior measurements,[9,12,25] we observe significantly reduced hysteresis in the thermal conductivity during heating and cooling cycles. We also perform the first demonstration of FDPR measurements on a thin film over a wide modulation-frequency bandwidth; we model the laser-induced charge transport as ambipolar diffusion in which electrons and holes diffuse according to their density gradients before recombination. We observe a significant change in the ambipolar diffusivity across the transition, accompanied by weaker hysteresis. The suppressed hysteresis in both thermal and charge transport is attributed to geometric anisotropy in the thin-film architecture, where the domain size is constrained by the film thickness, limiting percolation in the out-of-plane direction. These findings demonstrate the power of a local probe to resolve the nanoscale phase separation that governs the dynamics of tunable MITs in thin-film correlated oxides.

In bulk single crystals of $NdNiO_3$, the MIT is accompanied by a subtle structural transition from orthorhombic (Pbnm) to monoclinic ($P2_1/n$) symmetry (Figure 1a, b);[5,7,26] the transition has a thermal hysteresis of ∼4 K. In epitaxial thin films, the hysteresis increases to ∼30 K due to epitaxial strain.[11,27] We synthesize thin-film $NdNiO_3$ using ozone-assisted molecular-beam epitaxy (MBE) for atomic-layer control of the film deposition (see Figures S1−S3). Electrical transport measurements of our thin-film sample show a sharp change from metallic to insulating behavior in bulk resistivity measurements upon cooling at T_{cool} = 91 K, and we observe the reverse change at T_{heat} = 124 K during heating (Figure 1c). The biaxial compressive strain imposed by the $LaAlO_3$ substrate lowers T_{MIT} by over 70 K, consistent with prior observations of strain-induced suppression of T_{MIT}.

We explore thermal and electronic transport through complementary techniques of FDTR and FDPR on the same sample. As illustrated in Figure 2a, to isolate the thermal response of the film, we perform FDTR measurements for a region coated with a gold transducer layer (Figures S2, S3), which immediately converts electronic excitations into heat and ensures that the measured change in reflectance $\Delta R(\omega)$ is based only on the thermal properties of the sample (see SI).[19,20] To measure charge transport, we perform FDPR measurements on an adjacent uncoated region of the same sample; the photoreflectance signal includes contributions from heat diffusion and charge transport. We then determine the ambipolar carrier diffusivity across the transition.

In FDTR, the thermoreflectance signal is proportional to the change in the surface temperature of the gold transducer. The relative phase between the oscillations of the thermoreflectance signal and the pump modulation exhibits a distinct frequency dependence in the metallic phase compared to the insulating phase (Figure 2b). According to the sensitivity analysis based on the Fourier heat conduction model, our FDTR measurement is exclusively sensitive to the out-of-plane thermal conductivity $\kappa_\perp$ (Figure 2d). At high modulation frequencies, the phase shifts toward zero with increasing $\kappa_\perp$, while at low modulation frequencies, it shifts to more negative values with increasing $\kappa_\perp$ (Figure 2b). This relationship suggests that the out-of-plane thermal conductivity of the metallic phase is higher than that of the insulating phase, as expected.

In FDPR, the photoreflectance from the bare sample is the sum of the carrier-induced and temperature-induced components, both of which are represented by complex numbers. As shown in Figure 2c, at higher modulation frequencies, the carrier contribution can lower the overall phase lag compared with the temperature contribution alone, as carrier diffusion typically occurs much faster than heat diffusion. The different phase curves in the metallic and insulating states, especially at high modulation frequencies, are closely related to the difference in the carrier part of the signal. From the sensitivity analysis in Figure 2e, we observe that the constant A_ρ that determines the magnitude of the carrier contribution to the signal, the carrier recombination time τ, and ambipolar diffusivity D_a are

https://doi.org/10.1021/acs.nanolett.5c04522
Nano Lett. 2026, 26, 4027−4033

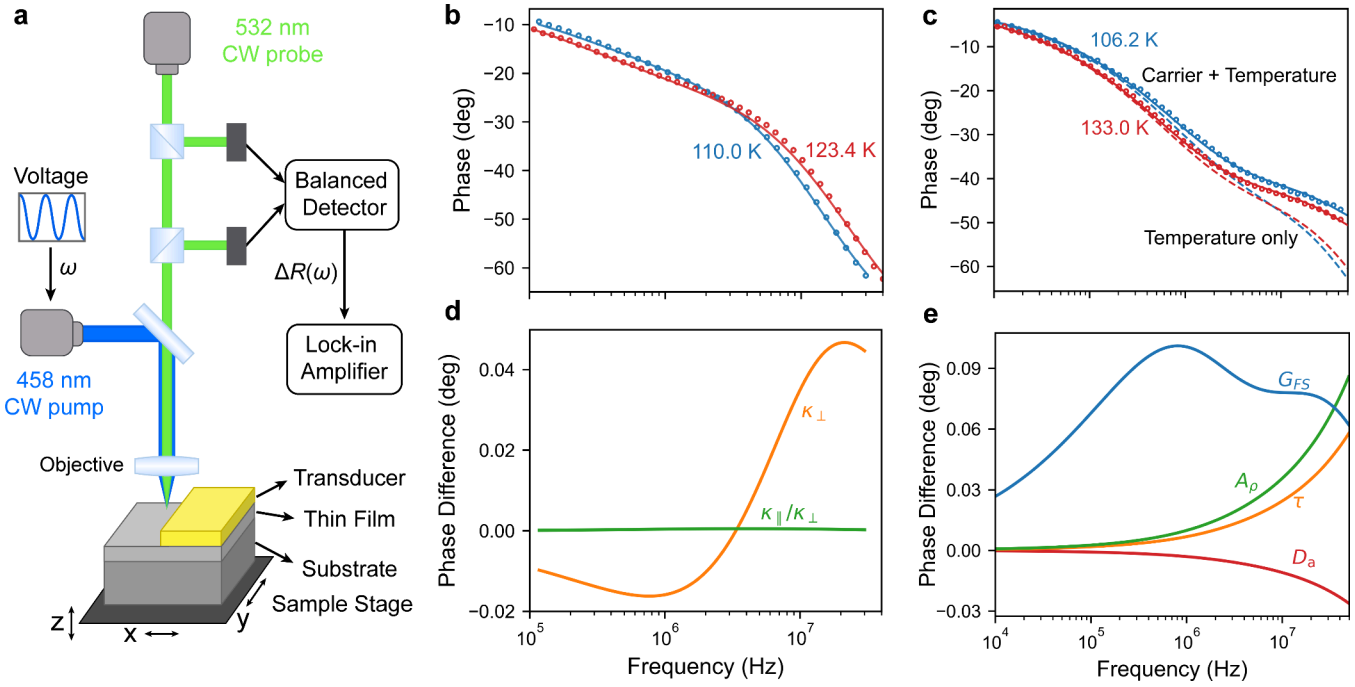

Figure 2. (a) Schematic of an integrated frequency-domain thermoreflectance (FDTR) and frequency-domain photoreflectance (FDPR) measurement setup. A continuous wave (CW) pump laser at 458 nm, power-modulated at a frequency $\omega/2\pi$, excites the sample. A CW probe laser at 532 nm reads out the perturbed reflectance. Both laser beams are focused to a 3 μm beam waist radius. The reference and reflected beams are first balanced and then detected by a balanced detector. The change in reflectance $\Delta R(\omega)$ is extracted from the output signal by a lock-in amplifier. FDTR and FDPR measurements are performed at the gold-coated (65.7 nm) and bare regions of the sample, respectively, with a piezoelectric stage being used to translate the sample in the xy-plane and to locate the beam focus along the z-axis. (b) FDTR phase data (circles) in the metallic (123.4 K) and insulating (110.0 K) phases, along with best fits using the Fourier heat conduction model (lines). (c) FDPR data in the metallic (133.0 K) and insulating (106.2 K) phases, along with best fits using the carrier and temperature model (solid lines); the phases of the temperature part of the signal are plotted in dashed lines. (d, e) Sensitivity analysis for FDTR (d) and FDPR (e) data fitting at 110.0 and 133.3 K, respectively. Specifically, $\kappa_{\parallel}$ and $\kappa_{\perp}$ correspond to the in-plane and out-of-plane thermal conductivity, respectively. G_{FS} is the thermal boundary conductance between the $NdNiO_3$ film and the $LaAlO_3$. A_ρ is related to the magnitude of the carrier contribution to the signal, τ is the carrier recombination time, and D_a is the ambipolar diffusivity. The phase difference is defined as the change in phase resulting from a + 1% relative increase in the corresponding variable.

correlated, allowing us to fit only one of these three parameters reliably. Given that D_a is substantially more susceptible to changes in transport than both A_ρ and τ, we fix the values of A_ρ and τ and treat D_a along with the thermal boundary conduction between the thin film and substrate, G_{FS}, as fitting variables (see Figures S7, S8).

Analyzing FDTR and FDPR data to extract transport properties of the thin film requires knowledge of the substrate properties. Therefore, we characterized the thermal properties of the $LaAlO_3$ substrate independently. We performed FDTR measurements on a $LaAlO_3$ substrate coated with a transducer layer (Figures S14, S15) and measured its thermal conductivity and heat capacity over the temperature range of 80−140 K (Figure 3a). The measured substrate heat capacity and thermal conductivity (Figure 3a) agree well with literature values for the heat capacity and thermal conductivity of $LaAlO_3$.[28] Notably, our approach enables the simultaneous determination of both thermal conductivity and heat capacity from a single measurement (Figure S13). This is achieved by varying the modulation frequency over a wide range: at higher frequencies, the thermoreflectance's phase has a positive correlation with both thermal conductivity and heat capacity, while at lower frequencies, its dependences on thermal conductivity and heat capacity have opposite signs.

We then fix the substrate thermal conductivity and heat capacity in our heat conduction model and determine the out-of-plane thermal conductivity ($\kappa_{\perp,tot}$) of the $NdNiO_3$ thin film. We perform heating and cooling measurements between 80−140 K. Simultaneously fitting both κ and C_p for the film is challenging because of the high uncertainty and because these parameters are strongly correlated. Therefore, we fix the film's heat capacity using a Debye model derived from bulk heat capacity measurements on $NdNiO_3$ (see Figure S16).[25,29] With only the film's thermal conductivity as a free parameter, we achieve stable fits with uncertainty <18%. Figure 3b shows the thermal conductivity κ of the thin film $NdNiO_3$ during cooling and heating cycles.

During cooling, the thermal conductivity $\kappa_{\perp,tot}$ of $NdNiO_3$ gradually decreases between 133.3 and 123.3 K. Between 123.3 and 110.0 K, it decreases more sharply by 33%, a phenomenon we describe as thermal switching. We compare the out-of-plane thermal conductivity to the predicted electronic contribution to the in-plane thermal conductivity using the Wiedemann−Franz law. It is important to recognize that the Wiedemann−Franz law can fail in correlated oxides,[30,31] where non-Fermi-liquid transport might emerge.[32] Consequently, we regard the predicted electronic thermal conductivity as a comparative indicator of in-plane heat transport. We calculate $\kappa_{\parallel,el} = L\sigma T$, where L is the Lorenz number, σ is the separately measured in-plane electrical conductivity (Figure 1a), and T is the temperature. In principle, we expect no anisotropy in the properties of bulk $NdNiO_3$, so we attribute the differences in thermal conductivity to finite scaling in the thin film limit.

https://doi.org/10.1021/acs.nanolett.5c04522
Nano Lett. 2026, 26, 4027−4033

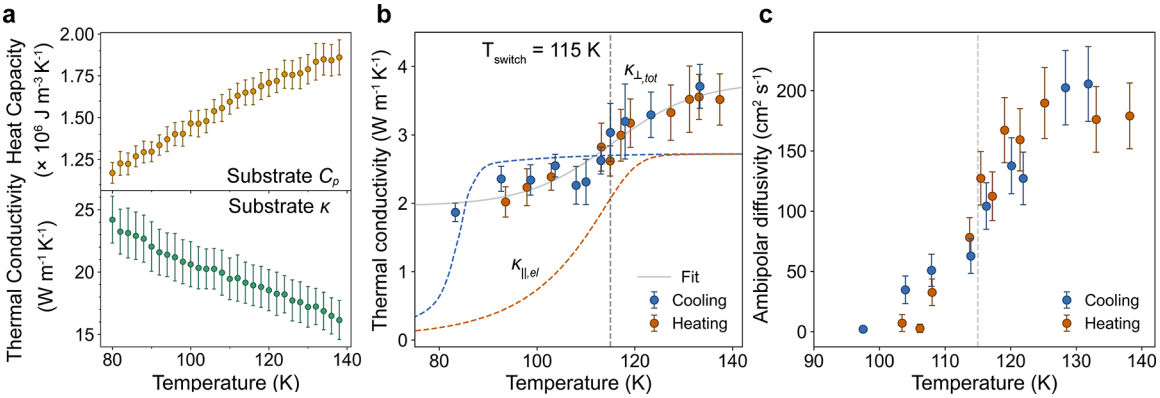

Figure 3. (a) The thermal conductivity and heat capacity of the substrate $LaAlO_3$ measured using FDTR. (b) Out-of-plane thermal conductivity, $\kappa_{\perp,tot}$, of thin film $NdNiO_3$ as a function of temperature, measured using FDTR over three cooling and two heating cycles (see Figure S5 for the full data and Table S1 for numerical values). The electronic contribution to in-plane thermal conductivity, $\kappa_{\parallel,el}$, predicted using the Wiedemann−Franz law is plotted as dashed lines. The hysteresis is weaker in the out-of-plane direction than in the in-plane direction, highlighting the anisotropy of the thin-film geometry. A modified logistic function, $f(T) = a[1 + e^{-b(T-T_{switch})}]^{-1} + c$, is used to fit the thermal conductivity trend (gray line). The thermal switching temperature T_{switch} is found to be 115 K. (c) The ambipolar diffusivity of $NdNiO_3$, measured using FDPR, across the metal−insulator transitions during cooling and heating. The dashed line corresponds to $T_{switch} = 115 \pm 4$ K, with the standard deviation obtained from a bootstrap analysis (Figure S6). Fixed parameters $A_\rho = 8 \times 10^{-25}$ m^3 K and $\tau = 0.11$ ns are chosen to minimize fitting residuals across all temperatures.

On cooling, we observe the onset of thermal switching in $\kappa_{\perp,tot}$ more than 20 K higher in temperature than in $\kappa_{\parallel,el}$. The heating curve of $\kappa_{\perp,tot}$ closely matches the cooling curve across the transition, suggesting that this transition temperature anisotropy arises from weak hysteresis in the out-of-plane direction. The hysteresis remains weak across different pump laser powers, eliminating the possibility that the laser reduces the hysteresis (Figure S9), and we can also rule out a photoinduced transition (Figure S11). Consistent with this behavior, the out-of-plane ambipolar diffusivity during heating and cooling from FDPR decreases sharply from 120 to 110 K and changes by much smaller amounts for $T < 110$ K (Figure 3c), which reinforces the idea that an electronic phase transition occurs at T_{switch}. The DC contribution of the reflectance from the bare sample, related to the dielectric constants of the thin film, also shows a sharp discontinuity at around 115 K, providing additional evidence for the electronic phase transition occurring near T_{switch} (Figure S12). Together, these measurements show that the transition temperature and the associated hysteresis measured in the out-of-plane direction differ substantially from those observed in the in-plane direction.

Both epitaxial strain and film thickness can tune the MIT in $NdNiO_3$, so we first consider whether differing strains in the out-of-plane direction can lead to anisotropic hysteresis. We expect that the film is under compressive strain in the in-plane direction due to the substrate, and therefore, it is under tensile strain in the out-of-plane direction.[33] While bulk $NdNiO_3$ has a hysteresis loop width of ∼4 K,[27] both compressive and tensile strain on thin films increase the hysteresis loop width to >10 K.[34] We therefore expect hysteresis in the in-plane and out-of-plane directions, and anisotropic strain effects should not eliminate hysteresis in the out-of-plane direction. To understand the origin of the discrepancy, we then consider the length scale of the FDTR and FDPR measurements compared to electrical resistivity measurements, understanding the dimensionality of the transition in the thin-film limit.

Previous imaging and local transport studies of the $NdNiO_3$ metal−insulator transition (MIT) show that the transition proceeds through mesoscale phase coexistence with insulating and metallic domains whose lateral size and morphology evolve strongly with temperature. Epitaxial strain has a strong influence on both the transition temperature and hysteresis width, so quantitative transition temperatures reported in the literature vary significantly between samples. In some epitaxial films, insulating domains form stripe-like patterns aligned with the substrate terracing, while in others such striping is not apparent. In the striped case, insulating domains are typically ∼200 nm wide and can extend much longer along the terrace direction,[10] whereas in nonstriped films the domains appear more irregular but retain a comparable characteristic lateral length scale.[9,35] Upon cooling through the MIT, isolated insulating domains nucleate at temperatures slightly above the nominal transition. As temperature decreases further, these insulating regions expand and connect with neighboring domains, progressively reducing the connectivity of the metallic network.[9,35] This loss of metallic connectivity drives the sharp increase in the resistivity observed on cooling. In films that exhibit stripe ordering, the insulating domain coverage increases with decreasing temperature and saturates at roughly 60%, while the striped morphology remains visible; metallic domains persist, but their lateral connectivity is strongly suppressed.[10] Upon heating, the evolution is different: insulating domains tend to melt from their edges and pinch off into smaller, disconnected regions, producing a domain distribution that is qualitatively distinct from that observed during cooling, even at the same insulating fraction. Because electrical transport depends on domain connectivity rather than phase fraction alone, this asymmetry in domain morphology and connectivity gives rise to observed macroscopic transport hysteresis.

The exact domain morphology in our films across the transition is not known, but we can estimate the length scale at which domains affect thermal and electrical transport. During heating, the effective metallic transport domains in the coexistence regime are typically 100−300 nm in size, as inferred from conductive atomic force microscopy (AFM) and related measurements.[9] Consistent with this scale, nanogap transport experiments report pronounced deviations from bulk hysteresis behavior for gap sizes in the range of ∼40−150 nm, where resistance drops abruptly when a single metallic domain bridges the contacts.[11] These characteristic length scales are comparable

https://doi.org/10.1021/acs.nanolett.5c04522
Nano Lett. 2026, 26, 4027−4033

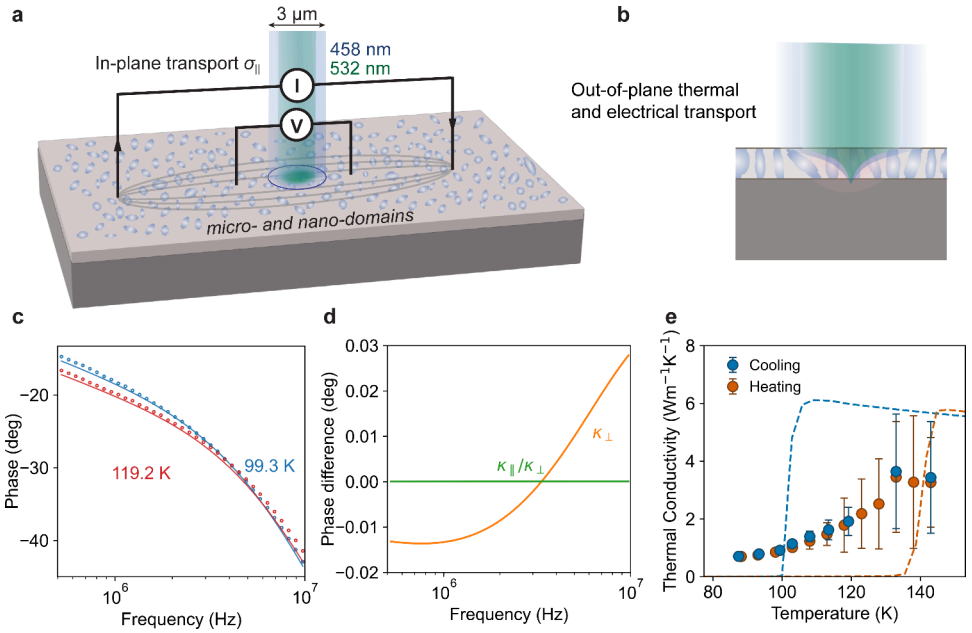

Figure 4. (a) Qualitative (not to scale) schematic representing the formation of insulating domains in $NdNiO_3$ near the phase transition temperature. FDPR probes out-of-plane electron transport on a length scale covering several domains, whereas the electrical resistance measurement aggregates in-plane contributions from electrons percolating across on the order of 10^3 domains. (b) Cross-sectional view of the beam penetration and domain formation (not to scale). Domains form instantaneously across the film thickness, directly creating single-phase transport channels without metal−insulator interfaces; hence, out-of-plane thermal and electron transport exhibits low hysteresis. (c) Phase lag data as a function of modulation frequency for the metallic (red) and insulating (blue) phases, together with best-fit model curves, for the 20.6 nm sample. (d) Sensitivity analysis for phase lag best fits at 133 K. A 1% increase in thermal conductivity produces negligible changes for the in-plane component. As with the 57.5 nm sample, the sensitivity to the in-plane thermal conductivity is nearly zero, while the sensitivity to the out-of-plane thermal conductivity is reduced. This reduction arises from the decreased film thickness and the correspondingly lower thermal resistance. (e) Out-of-plane thermal conductivity as a function of temperature, extracted from best-fit phase lag curves. Wiedemann−Franz law predictions for the electron contribution to in-plane thermal conductivity are overlaid (dashed lines). Minimal hysteresis is again observed in the out-of-plane thermal conductivity between the cooling and heating measurements, consistent with the 57.5 nm film.

to our film thickness (57.5 nm), suggesting that out-of-plane transport in thin films is governed by the formation of vertically continuous metallic paths rather than by in-plane percolation (Figure 4b). Consequently, out-of-plane transport is not as susceptible to domain connectivity, which changes the hysteresis. The FDTR/FDPR measurements probe reflectance over a spot size of ~3 μm. At these length scales, the measurement aggregates over hundreds of lateral domains within the coexistence regime (Figure 4a). As a result, abrupt resistivity or conductivity changes associated with the nucleation or percolation of individual metallic domains in the out-of-plane direction are averaged out, creating a smooth change in thermal and electrical transport without hysteresis.

This phenomenon is further corroborated by another measurement on a 20.6 nm thick $NdNiO_3$ film on $LaAlO_3$, also synthesized with MBE (Figure S10). This thinner film demonstrates a similar lack of hysteresis in the out-of-plane thermal conductivity. Figure 4c shows phase lag data and the best fits for metallic and insulating states. The sensitivity analysis (Figure 4d) shows that FDTR is less sensitive to this sample's out-of-plane thermal conductivity, $\kappa_{\perp}$, than to that of the 57.5 nm sample, as the 20.6 nm film has a lower thermal resistance. Still, we observe no hysteresis in the out-of-plane thermal conductivity measurements (Figure 4e). This result matches that of the 57.5 nm film, again suggesting a lack of percolation in the out-of-plane direction. We can therefore conclude that the anisotropy in the hysteresis is common to $NdNiO_3$ films of similar thicknesses to the 57.5 nm sample.

FDTR and FDPR in a thin-film geometry are uniquely sensitive to domain emergence in a phase transition, capturing the early onset of localized phase separation that precedes changes in the macroscopic properties. Although the diffraction limit prevents us from directly resolving the thermal conductivity of a single domain or right at the interface, our approach uniquely provides access to the cross-plane thermal conductivity, which, when combined with the mapped domain structures reported in previous studies,[10,26,35,36] allows us to understand how domains govern transport properties.

Our study reveals a microscopic, domain-mediated phase transition in $NdNiO_3$ preceding the MIT transition observed via bulk transport measurement. Thermal switching occurs at a temperature significantly above the metal−insulator transition identified by in-plane electrical transport measurements, with significantly reduced hysteresis. The thin-film geometry plays a significant role in the reduced hysteresis as the length scale of the domains formed during the transition is larger than the film thickness, allowing us to reduce percolation across domains in the out-of-plane direction. While much research on $NdNiO_3$ has been dedicated to tuning the hysteresis and transition temperature of the MIT, the anisotropy of the thin-film geometry has yet to be addressed and presents another way to tune the properties of the MIT. These results position $NdNiO_3$ thin films within a growing class of correlated oxides that exhibit nontrivial transport behavior across electronic phase transitions. Violations of the Wiedemann−Franz law observed in VO_2 nanowires near the MIT[31] suggest the involvement of unconventional quasiparticles or other strongly correlated

https://doi.org/10.1021/acs.nanolett.5c04522
Nano Lett. 2026, 26, 4027−4033

transport phenomena.[37] The unusual behavior of the reduced dimensionality in VO_2 nanowires highlights the macroscopic effects of fundamental length scales in correlated oxides with phase transitions. Our findings open new avenues for exploring the role of geometrical confinement and domain structure in such materials, advancing $NdNiO_3$ thin films as compelling candidates for realizing passive thermal switches and nonvolatile memristors.

Our work demonstrates that FDTR and FDPR offer unique capabilities for probing phase transitions in thin films where the domain sizes exceed the film thickness. In contrast to bulk resistivity, which probes in-plane transport percolating across many domains, our reflectance-based measurements are more sensitive to the local emergence and distribution of metallic and insulating domains. FDTR measurements in ultrathin films, therefore, primarily average transport across single domains, minimizing percolative effects and hysteresis. The sharp features observed in both thermal transport and ambipolar diffusivity near T_{switch} with weak hysteresis confirm the differences in the measurement due to the geometry of FDTR and FDPR. These insights demonstrate that FDTR is a powerful probe of phase transitions in complex oxides, enabling access to out-of-plane transport properties in regimes inaccessible to traditional bulk methods.

Beyond this central result, we introduce several methodological advances. We demonstrate that FDTR can simultaneously measure the thermal conductivity and heat capacity of a bulk substrate material (in this case, $LaAlO_3$) across a wide temperature range. We also report the first use of FDPR to extract ambipolar carrier diffusivity in a thin film system. The observed drop in D_a across the same temperature range as the thermal transition confirms the coevolution of electronic and thermal transport across the MIT. This combined FDTR/FDPR framework opens avenues for studying nanoscale phase transitions, domain dynamics, and anisotropic transport in complex oxides, both in equilibrium and under external stimuli such as strain or electric fields.

■ ASSOCIATED CONTENT

Supporting Information

The Supporting Information is available free of charge at https://pubs.acs.org/doi/10.1021/acs.nanolett.5c04522.

X-ray diffraction and X-ray reflectivity of $NdNiO_3$, X-ray reflectivity of the transducer layer, AFM of $NdNiO_3$, full derivation of the carrier and temperature model for FDPR signals, and data analysis (PDF)

■ AUTHOR INFORMATION

Corresponding Authors

Jarad A. Mason − *Department of Chemistry and Chemical Biology, Harvard University, Cambridge, Massachusetts 02138, United States;* orcid.org/0000-0003-0328-7775; Email: mason@chemistry.harvard.edu

Qichen Song − *Department of Chemistry and Chemical Biology, Harvard University, Cambridge, Massachusetts 02138, United States;* orcid.org/0000-0002-1090-4068; Email: qichensong@g.harvard.edu

Julia A. Mundy − *Department of Physics, Harvard University, Cambridge, Massachusetts 02138, United States; John A. Paulson School of Engineering and Applied Sciences, Harvard University, Cambridge, Massachusetts 02138, United States;* orcid.org/0000-0001-8454-0124; Email: mundy@fas.harvard.edu

Authors

Lucy S. Nathwani − *Department of Physics, Harvard University, Cambridge, Massachusetts 02138, United States;* orcid.org/0009-0001-5002-3812

Anne Ruperto − *Department of Physics, Harvard University, Cambridge, Massachusetts 02138, United States*

Ashvini Vallipuram − *Department of Physics, Harvard University, Cambridge, Massachusetts 02138, United States;* orcid.org/0009-0003-8895-4289

Abigail Y. Jiang − *John A. Paulson School of Engineering and Applied Sciences, Harvard University, Cambridge, Massachusetts 02138, United States; Department of Physics, Harvard University, Cambridge, Massachusetts 02138, United States;* orcid.org/0000-0001-8003-8380

Grace A. Pan − *Department of Physics, Harvard University, Cambridge, Massachusetts 02138, United States*

Dan Ferenc Segedin − *Department of Physics, Harvard University, Cambridge, Massachusetts 02138, United States;* orcid.org/0000-0001-7162-8100

Ari B. Turkiewicz − *Department of Physics, Harvard University, Cambridge, Massachusetts 02138, United States;* orcid.org/0000-0001-5729-0289

Charles M. Brooks − *Department of Physics, Harvard University, Cambridge, Massachusetts 02138, United States*

Complete contact information is available at: https://pubs.acs.org/10.1021/acs.nanolett.5c04522

Notes

The authors declare no competing financial interest.

■ ACKNOWLEDGMENTS

The authors thank Aaron J. Schmidt for helpful discussions. L.S.N. thanks Suzanne Smith and Jennifer Hoffman for their feedback on the manuscript. This project was primarily supported by the U.S. Department of Energy, Office of Basic Energy Sciences, Division of Materials Sciences and Engineering, under Award No. DE-SC0021925. We also acknowledge support from the National Science Foundation with Award No. DMR-2323970. This work was performed in part at the Harvard University Center for Nanoscale Systems (CNS); a member of the National Nanotechnology Coordinated Infrastructure Network (NNCI), which is supported by the National Science Foundation under NSF Award No. ECCS-2025158. Q.S., L.S.N., and A.R. acknowledge support from the Harvard Quantum Initiative. A.Y.J., G.A.P., and D.F.S. acknowledge support from the NSF Graduate Research Fellowship Grant DGE-1745303. A.Y.J. and G.A.P. were also supported by the Paul & Daisy Soros Fellowship for New Americans and A.Y.J. by the Ford Foundation. J.A.M. acknowledges funding from the Star Friedman Fund at Harvard University. L.S.N. and A.R. acknowledge support from the Herchel Smith Undergraduate Science Research Program. Generative A.I. was used in the code to create plots for the figures.

■ REFERENCES

(1) Wen, C.; Feng, L.; Li, Z.; Bai, J.; Wang, S.; Gao, X.; Wang, J.; Yao, W. A review of the preparation, properties and applications of VO_2 thin films with the reversible phase transition. *Frontiers in Materials* **2024**, *11*, 1341518.

(2) Haddad, E.; Kruzelecky, R. V.; Murzionak, P.; Jamroz, W.; Tagziria, K.; Chaker, M.; Ledrogoff, B. Review of the VO_2 smart material applications with emphasis on its use for spacecraft thermal control. *Frontiers in Materials* **2022**, *9*, 1013848.
(3) Xia, Q.; Yang, J. J. Memristive crossbar arrays for brain-inspired computing. *Nat. Mater.* **2019**, *18*, 309−323.
(4) Imada, M.; Fujimori, A.; Tokura, Y. Metal-insulator transitions. *Rev. Mod. Phys.* **1998**, *70*, 1039−1263.
(5) Catalano, S.; Gibert, M.; Fowlie, J.; Íñiguez, J.; Triscone, J.-M.; Kreisel, J. Rare-earth nickelates $RNiO_3$: thin films and heterostructures. *Rep. Prog. Phys.* **2018**, *81*, 046501.
(6) Alonso, J. A.; Martínez-Lope, M. J.; Casais, M. T.; García-Muñoz, J. L.; Fernández-Díaz, M. T. Room-temperature monoclinic distortion due to charge disproportionation in R NiO 3 perovskites with small rare-earth cations (R = Ho, Y, Er, Tm, Yb, and Lu): A neutron diffraction study. *Phys. Rev. B* **2000**, *61*, 1756−1763.
(7) García-Muñoz, J. L.; Aranda, M. A. G.; Alonso, J. A.; Martínez-Lope, M. J. Structure and charge order in the antiferromagnetic band-insulating phase of $NdNiO_3$. *Phys. Rev. B* **2009**, *79*, 134432.
(8) Liu, J.; Kargarian, M.; Kareev, M.; Gray, B.; Ryan, P. J.; Cruz, A.; Tahir, N.; Chuang, Y.-D.; Guo, J.; Rondinelli, J. M.; Freeland, J. W.; Fiete, G. A.; Chakhalian, J. Heterointerface engineered electronic and magnetic phases of $NdNiO_3$ thin films. *Nat. Commun.* **2013**, *4*, 2714.
(9) Preziosi, D.; Lopez-Mir, L.; Li, X.; Cornelissen, T.; Lee, J. H.; Trier, F.; Bouzehouane, K.; Valencia, S.; Gloter, A.; Barthélémy, A.; Bibes, M. Direct mapping of phase separation across the metal−insulator transition of $NdNiO_3$. *Nano Lett.* **2018**, *18*, 2226−2232.
(10) Mattoni, G.; Zubko, P.; Maccherozzi, F.; van der Torren, A.; Boltje, D. B.; Hadjimichael, M.; Manca, N.; Catalano, S.; Gibert, M.; Liu, Y.; Aarts, J.; Triscone, J.-M.; Dhesi, S. S.; Caviglia, A. D. Striped nanoscale phase separation at the metal−insulator transition of heteroepitaxial nickelates. *Nat. Commun.* **2016**, *7*, 13141.
(11) Lee, J. H.; Trier, F.; Cornelissen, T.; Preziosi, D.; Bouzehouane, K.; Fusil, S.; Valencia, S.; Bibes, M. Imaging and Harnessing Percolation at the Metal−Insulator Transition of $NdNiO_3$ Nanogaps. *Nano Lett.* **2019**, *19*, 7801−7805.
(12) Zhang, J. Y.; Kim, H.; Mikheev, E.; Hauser, A. J.; Stemmer, S. Key role of lattice symmetry in the metal-insulator transition of $NdNiO_3$ films. *Sci. Rep.* **2016**, *6*, 23652.
(13) Laffez, P.; Lebedev, O. I.; Ruello, P.; Desfeux, R.; Banerjee, G.; Capon, F. Evidence of strain induced structural change in hetero-epitaxial $NdNiO_3$ thin films with metal-insulator transition. *European Physical Journal Applied Physics* **2004**, *25*, 25−31.
(14) Wang, L.; Dash, S.; Chang, L.; You, L.; Feng, Y.; He, X.; Jin, K.-j.; Zhou, Y.; Ong, H. G.; Ren, P.; Wang, S.; Chen, L.; Wang, J. Oxygen Vacancy Induced Room-Temperature Metal−Insulator Transition in Nickelate Films and Its Potential Application in Photovoltaics. *ACS Appl. Mater. Interfaces* **2016**, *8*, 9769−9776.
(15) Shi, Y.; Chen, L.-Q. Thermodynamics of strain engineering in $RNiO_3$ (R = Sm, Nd). *Phys. Rev. B* **2024**, *110*, 205117.
(16) Grissonnanche, G.; Pan, G. A.; LaBollita, H.; Segedin, D. F.; Song, Q.; Paik, H.; Brooks, C. M.; Beauchesne-Blanchet, E.; Santana González, J. L.; Botana, A. S.; Mundy, J. A.; Ramshaw, B. J. Electronic band structure of a superconducting nickelate probed by the Seebeck coefficient in the disordered limit. *Physical Review X* **2024**, *14*, 041021.
(17) Cahill, D. G. Thermal conductivity measurement from 30 to 750 K: the 3ω method. *Rev. Sci. Instrum.* **1990**, *61*, 802−808.
(18) Oh, D.-W.; Ko, C.; Ramanathan, S.; Cahill, D. G. Thermal conductivity and dynamic heat capacity across the metal-insulator transition in thin film VO_2. *Appl. Phys. Lett.* **2010**, *96*, 151906.
(19) Yang, J.; Maragliano, C.; Schmidt, A. J. Thermal property microscopy with frequency domain thermoreflectance. *Rev. Sci. Instrum.* **2013**, *84*, 104904.
(20) Schmidt, A. J.; Cheaito, R.; Chiesa, M. A frequency-domain thermoreflectance method for the characterization of thermal properties. *Rev. Sci. Instrum.* **2009**, *80*, 094901.
(21) Ziade, E.; Schmidt, A. Imaging Thermal Transport in Graphene. *Journal of Heat Transfer* **2015**, *137*, 020901.
(22) Akura, Y.; Ikeda, Y.; Matsunaga, Y.; Shimofuri, M.; Banerjee, A.; Tsuchiya, T.; Hirotani, J. Frequency-domain thermoreflectance with beam offset without the spot distortion for accurate thermal conductivity measurement of anisotropic materials. *Rev. Sci. Instrum.* **2025**, *96*, 014902.
(23) Song, Q.; Warkander, S.; Huberman, S. C. Probing carrier and phonon transport in semiconductors all at once through frequency-domain photoreflectance. *Physical Review Applied* **2024**, *21*, 034044.
(24) Gonzalez-Munoz, S.; Agarwal, K.; Castanon, E. G.; Kudrynskyi, Z. R.; Kovalyuk, Z. D.; Spièce, J.; Kazakova, O.; Patanè, A.; Kolosov, O. V. Direct Measurements of Anisotropic Thermal Transport in γ-InSe Nanolayers via Cross-Sectional Scanning Thermal Microscopy. *Advanced Materials Interfaces* **2023**, *10*, 2300081.
(25) Hooda, M.; Yadav, C. Electronic properties and the nature of metal−insulator transition in $NdNiO_3$ prepared at ambient oxygen pressure. *Physica B: Condensed Matter* **2016**, *491*, 31−36.
(26) Gomes, M. M.; Manjunath, B.; Vilarinho, R.; Bassou, A. A.; Silva, B.; Oliveira, J.; Çaha, I.; Deepak, F. L.; Almeida, B.; Almeida, A.; Kreisel, J.; Tavares, P. B.; Íñiguez, J.; Moreira, J. A. Structural percolation evolution throughout the metal-to-insulator transition in $NdNiO_3$. *Phys. Rev. B* **2024**, *109*, 224109.
(27) Catalan, G.; Bowman, R. M.; Gregg, J. M. Metal-insulator transitions in $NdNiO_3$ thin films. *Phys. Rev. B* **2000**, *62*, 7892−7900.
(28) Schnelle, W.; Fischer, R.; Gmelin, E. Specific heat capacity and thermal conductivity of $NdGaO_3$ and $LaAlO_3$ single crystals at low temperatures. *J. Phys. D: Appl. Phys.* **2001**, *34*, 846−851.
(29) Barbeta, V. B.; Jardim, R. F.; Torikachvili, M. S.; Escote, M. T.; Cordero, F.; Pontes, F. M.; Trequattrini, F. Metal-insulator transition in $Nd_{1-x}Eu_xNiO_3$ probed by specific heat and anelastic measurements. *J. Appl. Phys.* **2011**, *109*, 07E115.
(30) Ronning, F.; Hill, R. W.; Sutherland, M.; Hawthorn, D. G.; Tanatar, M. A.; Paglione, J.; Taillefer, L.; Graf, M. J.; Perry, R. S.; Maeno, Y.; Mackenzie, A. P. Thermal Conductivity in the Vicinity of the Quantum Critical End Point in $Sr_3Ru_2O_7$. *Phys. Rev. Lett.* **2006**, *97*, 067005.
(31) Lee, S.; Hippalgaonkar, K.; Yang, F.; Hong, J.; Ko, C.; Suh, J.; Liu, K.; Wang, K.; Urban, J. J.; Zhang, X.; Dames, C.; Hartnoll, S. A.; Delaire, O.; Wu, J. Anomalously low electronic thermal conductivity in metallic vanadium dioxide. *Science* **2017**, *355*, 371−374.
(32) Mahajan, R.; Barkeshli, M.; Hartnoll, S. A. Non-Fermi liquids and the Wiedemann-Franz law. *Phys. Rev. B* **2013**, *88*, 125107.
(33) Wang, L.; Ju, S.; You, L.; Qi, Y.; Guo, Y.-w.; Ren, P.; Zhou, Y.; Wang, J. Competition between strain and dimensionality effects on the electronic phase transitions in $NdNiO_3$ films. *Sci. Rep.* **2016**, *5*, 18707.
(34) Scherwitzl, R.; Zubko, P.; Lezama, I. G.; Ono, S.; Morpurgo, A. F.; Catalan, G.; Triscone, J. Electric-Field Control of the Metal-Insulator Transition in Ultrathin $NdNiO_3$ Films. *Adv. Mater.* **2010**, *22*, 5517−5520.
(35) Bisht, R. S.; Samanta, S.; Raychaudhuri, A. K. Phase coexistence near the metal−insulator transition in a compressively strained $NdNiO_3$ film grown on $LaAlO_3$: Scanning tunneling, noise, and impedance spectroscopy studies. *Phys. Rev. B* **2017**, *95*, 115147.
(36) Li, J.; Pelliciari, J.; Mazzoli, C.; Catalano, S.; Simmons, F.; Sadowski, J. T.; Levitan, A.; Gibert, M.; Carlson, E.; Triscone, J.-M.; Wilkins, S.; Comin, R. Scale-invariant magnetic textures in the strongly correlated oxide NdNiO3. *Nat. Commun.* **2019**, *10*, 4568.
(37) Zhang, J.; Levenson-Falk, E. M.; Ramshaw, B. J.; Bonn, D. A.; Liang, R.; Hardy, W. N.; Hartnoll, S. A.; Kapitulnik, A. Anomalous thermal diffusivity in underdoped $YBa_2Cu_3O_{6+x}$. *Proc Natl Acad Sci U S A* **2017**, *114*, 5378−5383.

https://doi.org/10.1021/acs.nanolett.5c04522
Nano Lett. 2026, 26, 4027−4033